

# A Little Energy Goes a Long Way: Energy-Efficient, Accurate Conversion from Convolutional Neural Networks to Spiking Neural Networks

Dengyu Wu, Xinping Yi, and Xiaowei Huang

University of Liverpool, UK

{dengyu.wu,xinping.yi,xiaowei.huang}@liverpool.ac.uk

## Abstract

*Spiking neural networks (SNNs) offer an inherent ability to process spatial-temporal data, or in other words, real-world sensory data, but suffer from the difficulty of training high accuracy models. A major thread of research on SNNs is on converting a pre-trained convolutional neural network (CNN) to an SNN of the same structure. State-of-the-art conversion methods are approaching the accuracy limit, i.e., the near-zero accuracy loss of SNN against the original CNN. However, we note that this is made possible only when significantly more energy is consumed to process an input. In this paper, we argue that this trend of “energy for accuracy” is not necessary – a little energy can go a long way to achieve the near-zero accuracy loss. Specifically, we propose a novel CNN-to-SNN conversion method that is able to use a reasonably short spike train (e.g., 256 timesteps for CIFAR10 images) to achieve the near-zero accuracy loss. The new conversion method, named as explicit current control (ECC), contains three techniques (current normalisation, thresholding for residual elimination, and consistency maintenance for batch-normalisation), in order to explicitly control the currents flowing through the SNN when processing inputs. We implement ECC into a tool nicknamed SpKeras, which can conveniently import Keras CNN models and convert them into SNNs. We conduct an extensive set of experiments with the tool – working with VGG16 and various datasets such as CIFAR10 and CIFAR100 – and compare with state-of-the-art conversion methods. Results show that ECC is a promising method that can optimise over energy consumption and accuracy loss simultaneously.*

## 1. Introduction

As the third-generation artificial neural network, SNNs mimic biological neural networks by using spikes to transmit the information. It processes inputs, which are encoded as spike trains, sequentially and operates with much lower energy consumption than CNNs. The pioneering work

SpiNNaker [13], a neuromorphic computing platform based on SNNs, can run real-time billions of neurons to simulate human brain. The neuromorphic chips, such as TrueNorth [1], Loihi [3], and Tianji [14], are developed to directly implement SNNs, with now 10,000 neurons can be integrated on a single chip. The massively parallel and asynchronous design of neuromorphic chips can implement large-scale SNNs with low latency and low power consumption. Besides, through the combination with sensors, SNNs can be applied to edge computing, robotics, and other fields, to build low-power intelligent systems [15].

While promising, the training of SNNs has become a major challenge. Unlike CNNs which are trained by utilising stochastic gradient descent, SNNs work with binary signals – spikes – and do not have a straightforward way of obtaining gradients, although there are some recent attempts on this direction, see e.g., [11, 10]. A major thread of research on SNNs is to avoid the direct training, by converting a well-trained CNN to an SNN of the same structure. A few different approaches, such as [4, 16, 18, 5], have been proposed in the past few years. It is not surprising that there is an accuracy loss between SNNs and CNNs. For example, in [16, 18], the gap is between 0.15% - 2% for CIFAR10 networks. A recent work [18] shows that this gap can be further reduced if we use a sufficiently long (e.g., 1024 timesteps) spike train to encode an image input. It is well known that, a longer spike train will inevitably lead to higher latency, more spiking operations, and consume more energy. This situation was believed to be eased in [5], which claims that the length of spike train can be drastically shortened in order to achieve near-zero accuracy loss. However, as we suggested in this paper (Section 4.3), their threshold scaling method can easily lead to a significant increase on the spike-caused synaptic operations [16], or spike operations for short, which also lead to significant increase on the energy consumption. Therefore, state-of-the-art methods are on the trend of “energy for accuracy”.

In this paper, we suggest that the energy consumption and the accuracy loss need to be optimised simultaneously for a successful conversion. Figure 1 provides an illustra-

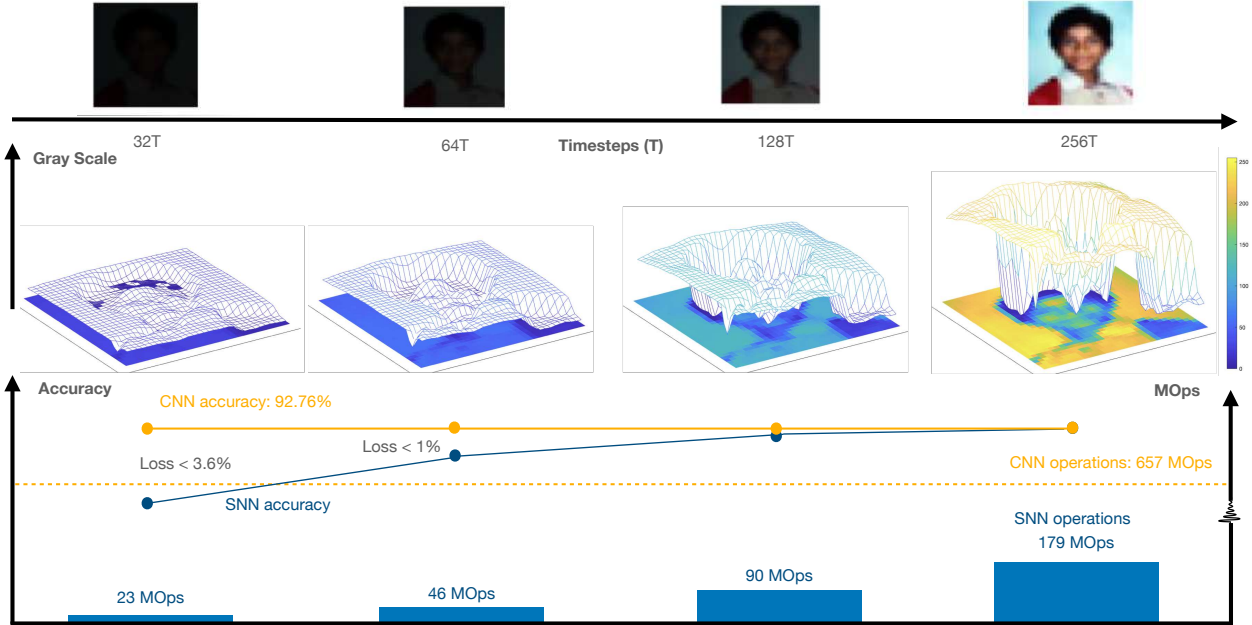


Figure 1: An illustrative diagram showing the changes of images (first row), energy contained in the spike train (second row), the accuracy loss (third row), and the number of spike operations (fourth row), with the change of timesteps in the spike train.

tive diagram showing what we believe the results should be. On the top row, we have an CIFAR-100 image (4th in the dataset) such that from right to left, it is gradually compressed by using one less bit width to represent the pixel value. For example, the top left image only has 5 bits, instead of the original 8 bits, to represent a pixel value. Visually, the impact on the image is that the gray scale information is gradually suppressed. In SNNs, these can be simulated as spike trains of different length, from 32 timesteps to 256 timesteps. The second row shows that, with the increase of the gray scale, the energy included in the spike trains increases, too. An ideal conversion method will require (1) as small as possible the number of spike operations (measured as MOps), (2) an almost linear increase of spike operations with respect to the length of spike train, (3) as small as possible the number of timesteps to achieve near-zero accuracy loss, (4) as small as possible the accuracy losses in general, and (5) an almost linear decrease on the accuracy loss with respect to the length of spike train. This is possible: the accuracy curve and spike operations in Figure 1 are generated by our proposed conversion method and meet the above requirements. State-of-the-art methods cannot achieve all these requirements, with [16] having too large the loss, [18] too many timesteps for near-zero accuracy loss, and [5] too many spike operations.

Methodologically, we believe that an explicit, and detailed, control on the currents flowing through the SNN may enable an optimisation for the two objectives (energy efficiency and near-zero accuracy loss) simultaneously. To sup-

port this view, we develop a unifying theoretical framework, which treats both weight normalisation [16] and threshold balancing [18] as special cases. More importantly, based on the framework, we develop a novel conversion method called explicit current control (ECC), which includes three techniques: current normalisation (CN) is to control the maximum number of spikes fed into the SNN, thresholding for residual elimination (TRE) is to reduce the residual membranes potential in the neurons, and consistency maintenance for batch-normalisation (CMB) is to reduce the inconsistency between CNN and SNN when converting batch-normalisation layer.

We implement the ECC method into a tool SpKeras<sup>1</sup> and conduct an extensive set of experiments to compare the performance with state-of-the-art methods [16, 18, 5]. The experimental results show that (1) comparing with [5, 18], ECC can achieve competitive performance in achieving the near-zero accuracy loss but require significantly less spike operations, (2) ECC only slightly increases the spiking operations over [16] but can significantly reduce the timesteps to achieve near-zero accuracy loss. That is, ECC minimises over two objectives – energy consumption and accuracy loss – simultaneously.

## 2. Related Work

Unlike CNNs which approximate continuous functions, SNNs process information through non-differentiable spikes. By this reason, the well-performed CNN training

<sup>1</sup>The tool is included in supplementary material.

	HR	SR	WN*	TB*	TS	ECC	BN**	MP	AP
Cao et al. [2], 2015	✓								✓
Diehl et al. [4], 2015	✓		✓						✓
Rueckauer et al. [16], 2017		✓	✓						
Sengupta et al. [18], 2019	✓			✓					✓
Han et al. [5], 2020		✓		✓	✓				✓
[this paper]		✓	✓	✓	✓	✓	✓		✓

Table 1: Comparison of Key Technical Ingredients (HR, SR, WN, TB, TS, ECC) and Workable Layers (BN, MP, AP) with the State-of-the-Art Methods. HR: hard reset; SR: reset by subtraction, or soft reset; WN: weight normalization; TB: threshold balancing; TS: threshold scaling; ECC: explicit current control; BN: batch normalization; MP: max-pooling; AP: average-pooling. \* As a contribution of this paper, in Section 3.2, we show that both WN and TB are special cases of our ECC framework. \*\* Among all methods, only those that can handle BN have bias terms in their pre-trained CNNs.

algorithm, backpropagation (BP) [9], cannot be directly applied to SNNs. A few attempts have been made to adapt the BP algorithm by approximating its forward propagation phase, when working with SNNs. It is shown in [11] that the BP algorithm can be applied on the statistics of spikes, so that the discrete spiking process is approximated as a continuous, differentiable function. Moreover, it is possible to use the sum of spikes over timesteps to transform the SNNs training into searching the best spiking rate in each timestep [10]. However, none of these attempts can achieve an accuracy that is close to CNNs.

To avoid direct training, a major research direction on SNNs is to convert pre-trained CNNs into SNNs of the same structure, so that SNNs can take advantage of the accuracy of CNNs. A number of conversion methods have been proposed in the past few years [2, 4, 16, 18, 5]. Table 1 provides an overview of these conversion methods, and the comparison with ours, from the aspects of technical ingredients and workable layers. At the beginning, most of the techniques, such as [2, 4], are based on hard reset (HR) spiking neurons, which are reset to fixed reset potential once its membrane potential exceeds the firing threshold. HR neurons are also used in some recent methods such as [18]. The main criticism on the HR neurons is its significant information loss during the SNN inference. Soft reset (SR) neurons are shown better in other works such as [16, 5].

Weight normalization (WN) is proposed in [4] and extended in [16] to regulate the spiking rate in order to reduce accuracy loss. The other technique, threshold balancing (TB), is proposed in [18] and extended in [5], to assign appropriate threshold to the spiking neurons to ensure that they operate in the linear (or almost linear) regime. In this paper, we show that both WN and TB are special cases of our theoretical framework (Section 3.2).

Another technique, called threshold scaling (TS), is suggested in [5]. However, as our experimental result shown in Figure 3c, the application of TS can lead to significant greater energy consumption (measured as MOps). On the other hand, the new method we propose in this paper, i.e.,

explicit current control (ECC), can achieve smaller accuracy loss and significantly less energy consumption.

We also note in Table 1 the differences in terms of workable layers in CNNs/SNNs for different methods. For example, batch-normalisation (BN) layer [6] is known important for the optimisation of CNNs [17], but only one existing method, i.e., [16], can work with it. Similarly for the bias values of neurons which are pervasive for CNNs. Actually, the consideration of BN is argued in [5] as the key reason for the higher accuracy loss in [16]. The results of this paper show that, we can keep both BN and bias when optimising the conversion, by maintaining the consistency between the behaviour of SNN and CNN.

Finally, we follow most SNN research to consider average pooling (AP) layer instead of max-pooling (MP) layer.

### 3. Explicit Current Control (ECC)

#### 3.1. Existing CNN-to-SNN Conversion

Without loss of generality, we consider a CNN model of  $N$  layers such that layer  $n$  has  $M^n$  neurons, for  $n \in \{1, 2, \dots, N\}$ . The output of the neuron  $i \in \{1, \dots, M^n\}$  at layer  $n$  with ReLU activation function is given by

$$a_i^n = \max \left\{ 0, \sum_{j=1}^{M^{n-1}} W_{ij}^n a_j^{n-1} + b_i^n \right\} \quad (1)$$

where  $W_{ij}^n$  is the weight between the neuron  $j$  at layer  $n-1$  and the neuron  $i$  at layer  $n$ ,  $b_i^n$  is the bias of the neuron  $i$  at layer  $n$ , and  $a_i^0$  is initialised as the input  $x_i$ .

The activation  $a_i^n$  indicates the contribution of the neuron to the CNN inference. For CNN-to-SNN conversion, the greater  $a_i^n$  is, the higher spiking rate will be, for the corresponding neuron on SNN. An explanation of a conversion method from CNNs to SNNs was first introduced in [16] by using data-based weight normalization.

The conversion method uses integrated-and-fire (IF) neuron to construct a rate-based SNN without leak and refractory time. To convert from a CNN, the spiking rate of each

neuron in SNN is related to the activation of its corresponding neuron in the CNN. An iterative algorithm based on the *reset by subtraction* mechanism is described below. The membrane potential  $V_i^n(t)$  of the neuron  $i$  at the layer  $n$  can be described as

$$V_i^n(t) = V_i^n(t-1) + Z_i^n(t) - \Theta_i^n(t)V_{thr}^n \quad (2)$$

where  $V_{thr}^n$  represents the threshold value of layer  $n$  and  $Z_i^n(t)$  is the input current to neuron  $i$  at layer  $n$  such that

$$Z_i^n(t) = \sum_{j=1}^{M^{n-1}} W_{ij}^n \Theta_j^{n-1}(t) + b_i^n \quad (3)$$

with  $\Theta_i^n(t)$  being a step function defined as

$$\Theta_i^n(t) = \begin{cases} 1, & \text{if } V_i^n(t) \geq V_{thr}^n \\ 0, & \text{otherwise.} \end{cases} \quad (4)$$

In particular, when the current  $V_i^n(t)$  reaches the threshold  $V_{thr}^n$ , the neuron  $i$  at layer  $n$  will generate a spike, indicated by the step function  $\Theta_i^n(t)$ , and the membrane potential  $V_i^n(t)$  will be reset immediately for the next timestep by subtracting the threshold.

### 3.2. A Unifying Theoretical Framework

The above CNN-to-SNN conversion method is designed specifically for weight normalisation [16], and cannot accommodate other conversion methods, e.g., threshold balancing [18]. We propose a novel theoretical framework for CNN-to-SNN conversion that covers both weight normalisation [16] and threshold balancing [18] as special cases. In particular, the proposed framework improves over [16] by adopting a thresholding mechanism to quantify the accumulated current into spikes in SNN, and extends the threshold balancing mechanism to be compatible with batch normalization and bias.

We will work with the spiking rate of each SNN neuron  $i$  at layer  $n$ , defined as  $r_i^n(t) = N_i^n(t)/t$ , where  $N_i^n(t)$  is the number of spikes generated in the first  $t$  timesteps by neuron  $i$  at layer  $n$ . We remark that, it is possible that  $r_i^n(t) > 1$ , i.e., multiple spikes in a single timesteps, in which case the latency is increased to process extra spikes.

Our framework is underpinned by Proposition 1.

**Proposition 1** *In the CNN-to-SNN conversion, if the first layer CNN activation  $a_i^1$  and the first layer SNN current  $Z_i^1(t)$  satisfy the following condition*

$$\frac{1}{T} \sum_{t=1}^T Z_i^1(t) = a_i^1, \quad (5)$$

where  $T$  is a predefined maximum timesteps, then the SNN spiking rate at time step  $t$  can be iteratively computed by

$$r_i^n(t) = \frac{1}{V_{thr}^n} \left( \sum_{j=1}^{M^{n-1}} W_{ij}^n r_j^{n-1}(t) + b_i^n \right) - \Delta_i^n(t) \quad (6)$$

with  $\Delta_i^n(t) \triangleq V_i^n(t)/tV_{thr}^n$  representing the residual spiking rate. Initially, the spiking rate of neuron  $i$  at the first layer is  $r_i^1(t) = a_i^1/V_{thr}^1 - \Delta_i^1(t)$ .

**Remark 1** The spiking rate in Equation (6) is a generalised form of those using weight normalisation (WN) [16] and threshold balancing (TB) [18]. When keeping  $V_{thr}^1 = 1$ , by normalising  $W_{ij}^n$  we obtain WN; when keeping  $W_{ij}^n$  unchanged, by normalising  $V_{thr}^n$  we obtain TB.

The condition in Equation (5) bridges between the activations in CNNs and the accumulated currents in SNNs, i.e., *within the duration of a spike train, the average accumulated current equals to the CNN activation*. This is key to our theoretical framework, and different from some previous conversion method such as [16], which bridges between activations and firing rates. This *activation-current association* is reasonable because it aligns with the intuitions that (i) given a fixed spiking rate, a greater CNN activation requires a greater accumulated current in the SNN; and (ii) given a pre-trained CNN, more input spikes lead to increased current in the SNN.

Proposition 1 suggests that an explicit, optimised control on the currents may bring benefits to the spiking rate (so as to reduce energy consumption) and the residual current (so as to reduce the accuracy loss) simultaneously. Firstly, a normalisation on the currents  $Z_i^n(t)$  is able to control the spike number, with its details being given in Section 3.3.1. Secondly, the error term  $\Delta_i^n(t)$  will accumulate in deeper layers, causing lower spiking rate in the output layer [16]. The thresholding technique in Section 3.3.2 will be able to reduce impact from such error. Thirdly, we need to maintain the consistency between CNN and SNN so that the above control can be effective, as in Section 3.3.3.

The input is encoded into spike train with Algorithm 1.

---

#### Algorithm 1: Input encoding algorithm

---

```

Input Pixel value  $X_i^0$ 
 $S_i^0 = []$  # spike train of neuron  $i$ 
 $\kappa_0 = 100$  # Set current amplification factor
 $Z_i^0 = \frac{\kappa_0 X_i^0}{\max(X_i^0)}$ 
 $V_{thr}^0 = \kappa_0$ 
 $V_i^0 = 0$  # Initialise membrane potential
 $\Theta_i^0 = 0$  # Initialise spike status
for 1 to  $T$  do
   $V_i^0 = V_i^0 + Z_i^0 - \Theta_i^0 V_{thr}^0$  ;
   $\Theta_i^0 = 0$  ;
   $\Theta_i^0 = V_i^0 > V_{thr}^0$  ;
   $S_i^0.append(\Theta_i^0)$ 
end
Output Spike train  $S_i^0$ 

```

---

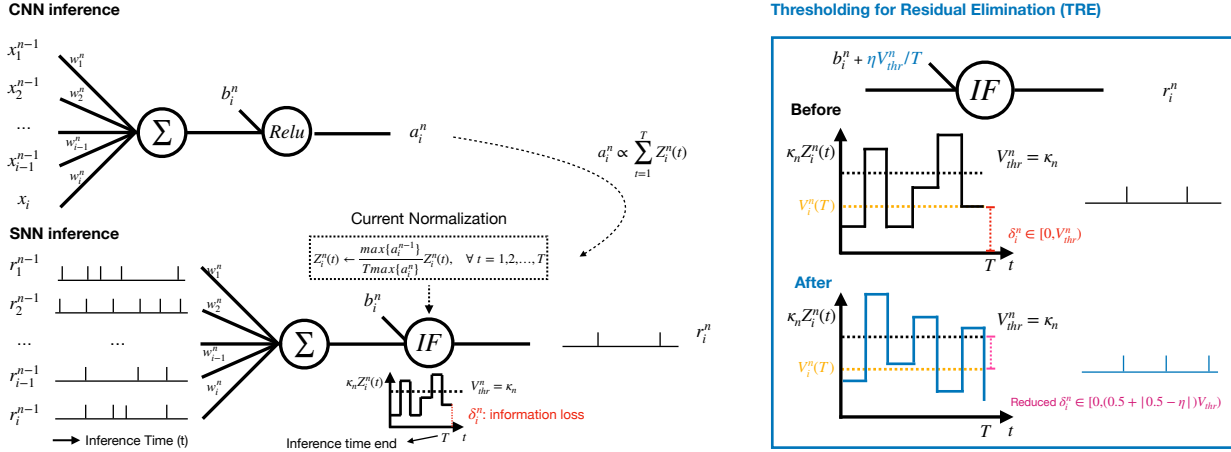


Figure 2: **Left:** Our proposed CNN-to-SNN conversion for the  $n$ -th layer with a current normalisation component and a thresholding mechanism. The activation  $a_i^n$  in the CNN (Top) is used for current normalisation in the SNN (Bottom). **Right:** The proposed Thresholding for Residual Elimination (TRE) and the illustration of error reduction by TRE.

### 3.3. ECC-Based Conversion Techniques

We develop three ECC-based techniques, including current normalisation (CN), thresholding for residual elimination (TRE), and consistency maintenance for batch-normalisation (CMB). Figure 2 illustrates CN and TRE, where the  $n$ -th layer of CNN is on the top and the corresponding conversed SNN layer is at the bottom. In the converted SNN layer, the sequences of spikes from the previous layer are aggregated, from which the current  $Z_i^n(t)$  is accumulated in the neurons, and normalised by a factor (see Equation (7) below) to ensure that the increase of current at each timestep is within the range of  $[0, 1]$ . The membrane potential  $V_i^n(t)$  is produced according to Equation (2), followed by a spike generating operation as in Equation (4) once  $V_i^n(t)$  exceeds the threshold  $V_{thr}^n = \kappa_n$ . The parameter  $\kappa_n$  is the current amplification factor, which will be explained in Section 3.3.1. The residual current  $\Delta_i^n$  at the end of spike train indicates the information loss in SNNs.

#### 3.3.1 Current Normalisation (CN)

At layer  $n$ , before spike generation, CN normalises the current  $Z_i^n(t)$  by letting

$$Z_i^n(t) \leftarrow \frac{\lambda_{n-1}}{T \lambda_n} Z_i^n(t), \quad \forall t = 1, \dots, T \quad (7)$$

where  $\lambda_n \triangleq \max_i \{a_i^n\}$  for  $n = 1, 2, \dots, N$ . We have  $\lambda_0 = 1$  when the input has been normalised into  $[0, 1]$  for every feature. The benefit of CN is two-fold:

- By CN, the maximum number of spikes fed into the SNN is under control, i.e., we can have a direct control on the energy consumption.

- It facilitates the use of a positive integer  $V_{thr}^n = \kappa_n$  as the threshold to quantify the current, which is amplified by factor of  $\kappa_n$ , for spike generation. In doing so, the neuron with maximum current can generate spike at every time step.

In Section 4, we set each  $\kappa_n = 100$  in each layer. However, conversion from floating point to fixed point will require different setting for each  $\kappa_n$  (section 4.4).

To achieve CN, the following conversion can be implemented to normalise weights and bias as follows.

$$W_{ij}^n \leftarrow \frac{\lambda_{n-1}}{\lambda_n} W_{ij}^n, \quad b_i^n \leftarrow \frac{\kappa_n b_i^n}{\lambda_n}, \quad V_{thr}^n \leftarrow \kappa_n. \quad (8)$$

Note that, the next layer will amplify the incoming current back to its original scale before its normalisation.

#### 3.3.2 Thresholding for Residual Elimination (TRE)

According to Equation (6), the error increment after conversion is mainly caused by the residual information,  $\delta_i^n(T) \in [0, V_{thr}^n]$ , which remains with each neuron after  $T$  timesteps and cannot be forwarded to higher layers. To mitigate such errors, we propose a technique TRE to keep  $\delta_i^n(T)$  under a certain threshold. In particular, we add extra current to each neuron in order to have  $\eta V_{thr}^n$  increment on each membrane potential, where  $\eta \in [0, 1)$ . Specifically, we update the bias term  $b_i^n$  of neuron  $i$  at layer  $n$  as follows

$$b_i^n(t) := b_i^n(t) + \eta V_{thr}^n / T \quad (9)$$

for every timestep  $t$ . Intuitively, we slightly increase synaptic bias for every neuron at every step, so that a small volume of current is pumped into the system continuously.

The following proposition says that this TRE technique will be able to achieve a reduction of error range, which directly lead to the improvement to the accuracy loss.

**Proposition 2** *Applying TRE will lead to*

$$\Theta_i^n(T) = \begin{cases} 1, & \text{if } V_i^n(T) > (1 - \eta)V_{thr}^n \\ 0, & \text{otherwise.} \end{cases} \quad (10)$$

for timestep  $T$ , as opposed to Equation (4). By achieving this, the possible range of errors is reduced from  $[0, V_{thr}^n)$  to  $[0, (0.5 + |\eta|)V_{thr}^n)$ .

We remark that, deploying TRE will increase at most one spike per neuron at the first layer and continue to affect the spiking rate at higher layers. This is the reason why we have slightly more spike operations than [16], as shown in Figure 3e. A typical value of  $\eta$  is 0.5.

### 3.3.3 Consistency Maintenance for Batchnormalisation (CMB)

Batch normalisation (BN) [7] accelerates the convergence of CNN training and improves the generalisation performance. The role of BN is to normalise output of its previous layer, which allows us to add the normalised information to weights and bias in the previous layer. We consider a conversion technique CMB to maintain the consistency between SNN and CNN in operating BN layer, by requiring a constant for numerical stability  $\epsilon$ , as follows.

$$\hat{W}_{ij}^n = \frac{\gamma_i^n}{\sqrt{\sigma_i^{n2} + \epsilon}} W_{ij}^n \quad (11)$$

$$\hat{b}_i^n = \frac{\gamma_i^n}{\sqrt{\sigma_i^{n2} + \epsilon}} (b_i^n - \mu_i^n) + \beta_i^n \quad (12)$$

where  $\gamma_i^n$  and  $\beta_i^n$  are two learned parameters,  $\mu_i^n$  and  $\sigma_i^n$  are mean and variance.  $\epsilon$  is platform dependent: for Tensorflow it is default as 0.001 and for PyTorch it is 0.00001. The conversion method in [16] does not consider  $\epsilon$ , and we found through a number of experiments that a certain amount of accuracy loss can be observed consistently. Figure 3a shows the capability of CMB in reducing the accuracy loss.

## 4. Experiment

We implement the ECC method into a software tool Sp-Keras and conduct an extensive set of experiments to validate it. We consider three categories of experiments. First, a simple ablation study is conducted to understand the contribution of individual techniques in ECC. Second, a number of experiments are conducted to compare ECC with state-of-the-art methods. Third, we study how the two hyper-parameters of ECC (hardware precision  $b$  and thresholding parameter  $\eta$ ) may affect the performance. Note that, we fix  $\kappa_n = 100$  and  $\epsilon = 0.001$  throughout the experiments.

For comparison with existing methods, Table 2 provides an overview of the methods to be compared in this section. ‘2017-SNN’ denotes the method proposed in [16]. ‘RMP-SNN(0.8)’ and ‘RMP-SNN(0.9)’ denote the method in [5], with different parameter 0.8 or 0.9 as co-efficient to  $V_{thr}$ . ‘ECC-SNN’ is the ECC method we propose in the previous section. We remark that, it is shown in [5] that its conversion method outperforms that of [18], so we need only compare with the method in [5]. Moreover, we may write ‘Method@ $nT$ ’ to represent the specific ‘Method’ when considering the spike trains of length  $n$ .

Before proceeding, we explain how to estimate energy consumption. For CNNs, it is estimated through the multiply-accumulate (MAC) operations

$$\text{MAC operations for CNNs} : \sum_{n=1}^N (2f_{in}^n + 1)M^n \quad (13)$$

where  $f_{in}^n$  is the number of input connections of the  $n$ -th layer. The number of MAC operations are fixed when the architecture of the network is determined. For SNNs, the synaptic operations are counted to estimate the energy consumption of SNNs [12, 16], as follows.

$$\text{Synaptic operations for SNNs} : \sum_{t=1}^T \sum_{n=1}^N f_{out}^n s^n \quad (14)$$

where  $f_{out}^n$  is the number of output connections and  $s^n$  is the average number of spikes per neuron, of the  $n$ -th layer.

### 4.1. Experimental Settings

We work with two classification benchmarks, CIFAR-10 and CIFAR-100, on the VGG-16 [19] architecture<sup>2</sup>, with the max-pooling layers replaced by average pooling layers for the latter being more accessible for SNNs. We trained CNNs using Tensorflow by having a batch-normalization layer after each convolutional layer. All the experiments are conducted on a CentOS Linux machine with two 2080Ti GPUs and 11 GB memory.

### 4.2. A Simple Ablation Study of ECC-SNN

Figure 3a shows the contributions of the three ingredients of ECC-SNN we introduced in this paper, i.e., CN, CMB, and TRE. We conduct experiment on VGG-16 network for CIFAR-10, by gradually including technical ingredients to see their respective impact on the accuracy loss. Figure 3a shows the histograms of the mean accuracy losses, over the 281–283th epochs. We can see that, every ingredient plays a role in reducing the accuracy loss, with the TRE and CN being slightly more effective than CMB. In the following, when mentioning ECC-SNN, we take all the three ingredients.

<sup>2</sup>We also conducted experiments on other architectures such as VGG-19, with the results similar as we report for VGG-16.

Method	Publication	Latency for near-zero accuracy loss	Energy consumption (measured with MOps)
2017-SNN	[16], 2017	1024 timesteps (Figure 3c)	<b>the best</b>
RMP-SNN(0.8)	[5], 2020	128 timesteps (Figure 3c), <b>the best</b>	significantly more than 2017/ECC-SNN (Figure 3c)
RMP-SNN(0.9)	[5], 2020	256 timesteps (Figure 3c)	significantly more than 2017/ECC-SNN (Figure 3c)
ECC-SNN	<b>this paper</b>	128 timesteps (Figure 3c), <b>the best</b>	<b>only slightly more than 2017-SNN</b> (Figure 3c, 3e)

Table 2: CNN-to-SNN conversion methods, and their corresponding publications, that are compared in the experiments. Also, we provide the main comparison results against two criteria: latency for near-zero accuracy loss and energy efficiency.

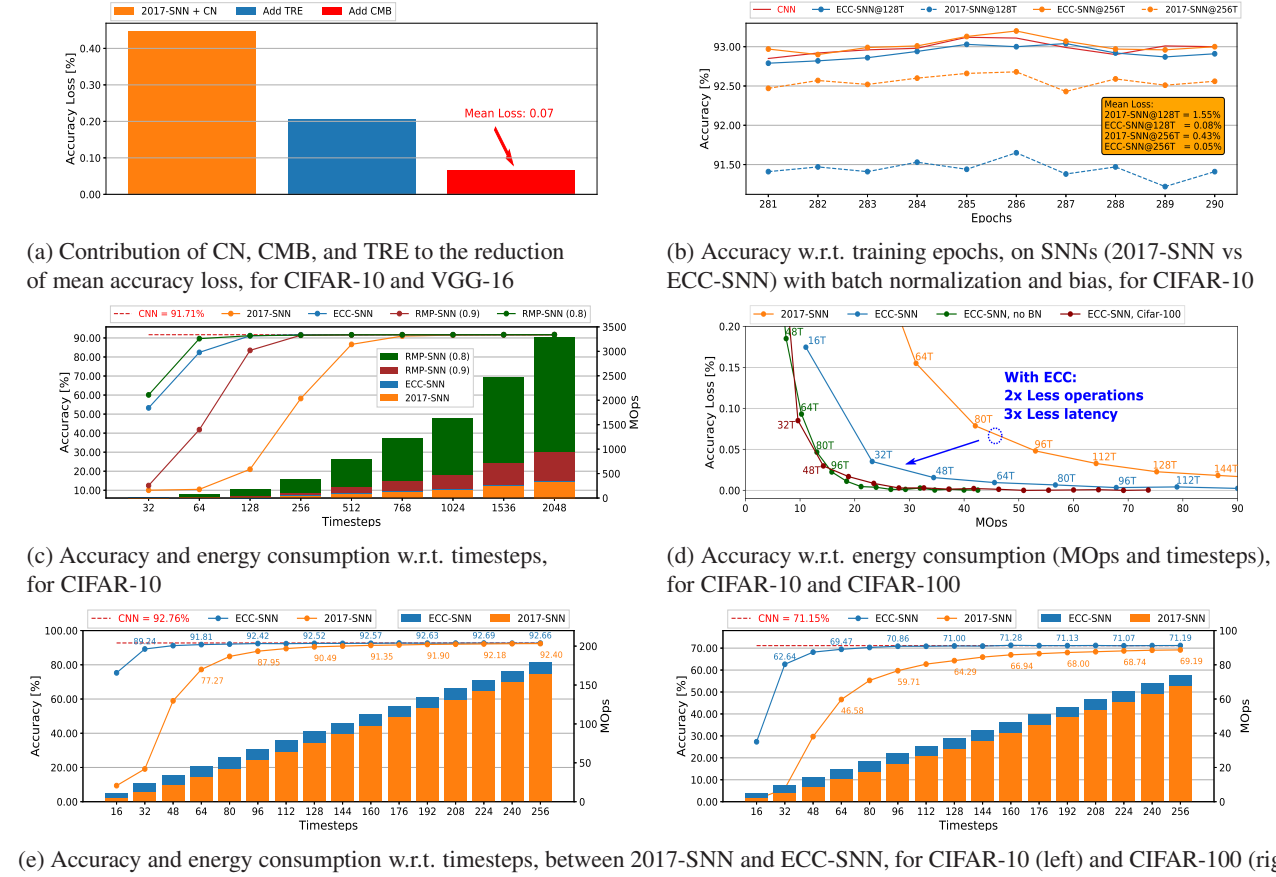


Figure 3: Comparisons of technical methods for CNN-to-SNN conversion

### 4.3. Comparisons with State-of-the-Art

Figure 3b shows the accuracy impact of small timesteps, for both ECC-SNN and 2017-SNN. We plot the accuracy of 10 epochs when the CNN training is almost converged, i.e., when the accuracy does not fluctuate significantly with the advance of epochs. For 2017-SNN, a smaller timestep may lead to significant performance drop. For example, the accuracy of 2017-SNN@256T is around 92.5%, while 2017-SNN@128T is around 91.5%, a 1% accuracy gap. On the other hand, ECC-SNN does not experience significant accuracy drop. *This observation supports our view that we may not need a significant amount of energy (here, the timesteps) to reach an acceptable level of accuracy loss.*

Figure 3c presents a comparison between 2017-SNN, RMP-SNN, and ECC-SNN on both accuracy and energy consumption with respect to the timesteps. First of all, both RMP-SNN and ECC-SNN perform better than 2017-SNN, in terms of the timestep to reach near-zero accuracy loss. Second, ECC-SNN is better than RMP-SNN(0.9) and competitive with RMP-SNN(0.8) in terms of reaching near-zero accuracy loss under certain latency. More specifically, both ECC-SNN and RMP-SNN(0.8) require 128 timesteps and RMP-SNN(0.9) requires 256 timesteps. Third, both RMP-SNN(0.8) and RMP-SNN(0.9) consume much more energy, measured with MOps, than ECC-SNN. Fourth, ECC-SNN does not consume significantly more energy than 2017-

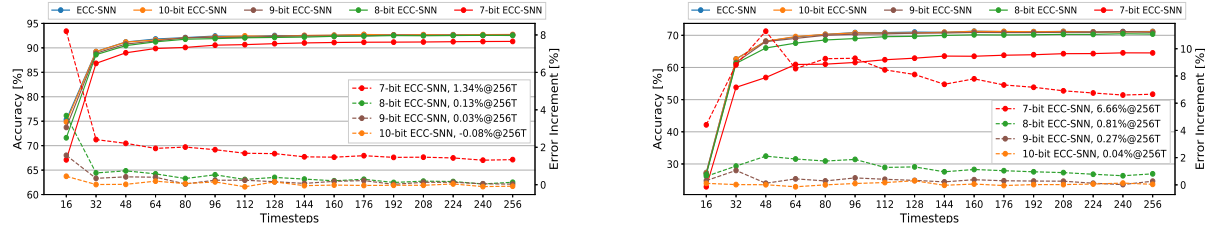


Figure 4: Accuracy and Error increment w.r.t. timesteps, for CIFAR-10 (left) and CIFAR-100 (right)

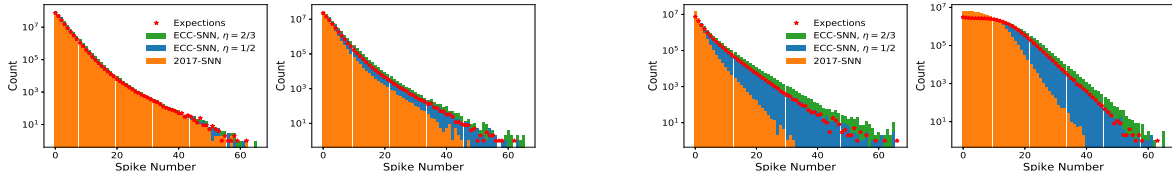


Figure 5: Spike count on 4th, 8th, 12th and 16th layer (from left to right) with 64 timesteps for CIFAR-100

SNN. The last point is further exhibited in Figure 3e, where we compare only ECC-SNN with 2017-SNN. We can see that, only a minor energy consumption increase from 2017-SNN to ECC-SNN, but ECC-SNN can achieve near-zero accuracy loss with much smaller timesteps. These observations reflect exactly the results we summarise in Table 2. That is, RMP-SNN(0.8) and ECC-SNN are the best in achieving near-zero accuracy loss with small timesteps, but RMP-SNN requires significantly more spike operations than the other two methods. Therefore, *ECC-SNN achieves the best when considering both energy consumption and latency for near-zero accuracy loss*.

Figure 3d considers the impact of working with batch-normalisation layer (and bias) and different datasets. We only compare with 2017-SNN because RMP-SNN does not work with BN. ECC-SNN can achieve similar accuracy performance by using 2x less operations and 3x less latency. ECC-SNN without BN can achieve lower operations, even though there is an increase on the latency. We can see that, with the same amount of energy (MOps), the consideration of BN on ECC-SNN leads to increased accuracy loss and reduced number of timesteps. On the other hand, considering larger dataset (CIFAR-100 vs CIFAR-10) will lead to a different situation, i.e., with the same amount of energy, CIFAR-100 leads to decreased accuracy loss and increased number of timesteps.

#### 4.4. Impact of Hyper-parameters of ECC-SNN

We consider how the hyper-parameter setting of ECC-SNN may affect the accuracy or spike operations. Figure 4 presents how the change on the number of bits to represent weights may affect the accuracy and error improvement. This is an important issue, as the SNNs will be deployed on neuromorphic chip, such as Loihi[3] and TrueNorth [1], or FPGA, which may have different configurations (For exam-

ple, Loihi can have weight precision at 1-9 bits). Floating-point data, both weights and threshold, can be simply converted into fixed-point data after CN by two steps: normalising the weights into range [-1,1] and scaling the threshold using the same normalisation factor, and then multiplied with  $2^b$ , where  $b$  is the bit width [8, 20]. We can see that, the reduction from 32-bit to 10-, 9-, 8- and 7-bit signed weights does lead to drop on the accuracy, but unless it goes to 7-bit, the accuracy loss is negligible. This shows that, *our ECC method is robust to hardware deployments*.

Figure 5 presents the spike count of hidden layers, for 2017-SNN and ECC-SNN with two different  $\eta$ , for CIFAR-100. We note that, on the shadow layers, the spike count increase of ECC-SNN over 2017-SNN is minor. It becomes more significant for deeper layers. The increased spikes help ECC-SNN to follow the expecting distribution more closely. The expectation curve is extracted by encoding CNNs activation in each layer directly, which is without impact of  $\Delta_i^n$  and represents the optimal case. When increasing  $\eta$  from 1/2 to 2/3, the spike count distribution deviates further from its expectation.

## 5. Conclusion

We develop a unifying theoretical framework to analyse the conversion from CNNs to SNNs and, based on the framework, develop a new conversion method ECC of three techniques (CN, TRE, CMB) to explicitly control the currents, so as to optimise accuracy loss and energy efficiency simultaneously. By comparing with state-of-the-art methods, we confirm the superior performance of our method. Moreover, we study the impact of hardware deployment on the performance of our method, and confirm that our method is robust to it, which will make our method applicable to wider applications.

## References

[1] F. Akopyan, J. Sawada, A. Cassidy, R. Alvarez-Icaza, J. Arthur, P. Merolla, N. Imam, Y. Nakamura, Nam Datta, P., G.J., and B. Taba. Truenorth: Design and tool flow of a 65 mw 1 million neuron programmable neurosynaptic chip. *IEEE transactions on computer-aided design of integrated circuits and systems*, 34(10):1537–1557, 2015. [1](#) [8](#)

[2] Y. Cao, Y. Chen, and D. Khosla. Spiking deep convolutional neural networks for energy-efficient object recognition. *International Journal of Computer Vision*, 113(1):54–66, 2015. [3](#)

[3] M. Davies, N. Srinivasa, T.H. Lin, G. Chinya, Y. Cao, S.H. Choday, G. Dimou, P. Joshi, N. Imam, S. Jain, and Y. Liao. Loihi: A neuromorphic manycore processor with on-chip learning. *IEEE Micro*, 38(1):82–99, 2018. [1](#) [8](#)

[4] P.U. Diehl, D. Neil, J. Binas, M. Cook, S.C. Liu, and M. Pfeiffer. Fast-classifying, high-accuracy spiking deep networks through weight and threshold balancing. *International Joint Conference on Neural Networks*, pages 1–8, 7 2015. [1](#) [3](#)

[5] B. Han, G. Srinivasan, and K. Roy. Rmp-snn: Residual membrane potential neuron for enabling deeper high-accuracy and low-latency spiking neural network. *Proceedings of the IEEE/CVF Conference on Computer Vision and Pattern Recognition*, pages 13558–13567, 2020. [1](#) [2](#) [3](#) [6](#) [7](#)

[6] Sergey Ioffe and Christian Szegedy. Batch normalization: Accelerating deep network training by reducing internal covariate shift. volume 37 of *Proceedings of Machine Learning Research*, pages 448–456, Lille, France, 07–09 Jul 2015. PMLR. [3](#)

[7] S. Ioffe and C Szegedy. Batch normalization: Accelerating deep network training by reducing internal covariate shift. *arXiv:1502.03167*, 2015. [6](#)

[8] X. Ju, B. Fang, R. Yan, X. Xu, and H. Tang. An fpga implementation of deep spiking neural networks for low-power and fast classification. *Neural computation*, 32(1):182–204, 2019. [8](#)

[9] Y. LeCun, B. Boser, J.S. Denker, D. Henderson, R.E. Howard, W. Hubbard, and L.D. Jackel. Backpropagation applied to handwritten zip code recognition. *Neural computation*, 4(1):541–551, 1989. [3](#)

[10] C. Lee, S.S. Sarwar, P. Panda, G. Srinivasan, and K. Roy. Enabling spike-based backpropagation for training deep neural network architectures. *Frontiers in Neuroscience*, 14, 2020. [1](#) [3](#)

[11] J.H. Lee, T. Delbruck, and M. Pfeiffer. Training deep spiking neural networks using backpropagation. *Frontiers in neuroscience*, 10:508, 11 2016. [1](#) [3](#)

[12] P.A. Merolla, J.V. Arthur, R. Alvarez-Icaza, A.S. Cassidy, J. Sawada, F. Akopyan, B.L. Jackson, N. Imam, C. Guo, Y. Nakamura, and B. Brezzo. A million spiking-neuron integrated circuit with a scalable communication network and interface. *Science*, 345(6197):668–673, 2014. [6](#)

[13] E. Painkras, L.A. Plana, J. Garside, S. Temple, S. Davidson, J. Pepper, D. Clark, C. Patterson, and S. Furber. Spinaker: A multi-core system-on-chip for massively-parallel neural net simulation. *NaIn Proceedings of the IEEE 2012 Custom Integrated Circuits Conference*, (7767):1–4, 9 2012. [1](#)

[14] J. Pei, L. Deng, S. Song, M. Zhao, Y. Zhang, S. Wu, G. Wang, Z. Zou, Z. Wu, W. He, and F. Chen. Towards artificial general intelligence with hybrid tianjic chip architecture. *Nature*, 572(7767):106–111, 2019. [1](#)

[15] M. Pfeiffer and T. Pfeil. Deep learning with spiking neurons: opportunities and challenges. *Frontiers in neuroscience*, 12:774, 2018. [1](#)

[16] B. Rueckauer, I.A. Lungu, M. Hu, Y. and Pfeiffer, and S.C. Liu. Conversion of continuous-valued deep networks to efficient event-driven networks for image classification. *Frontiers in neuroscience*, 11:682, 2017. [1](#) [2](#) [3](#) [4](#) [6](#) [7](#)

[17] Shibani Santurkar, Dimitris Tsipras, Andrew Ilyas, and Aleksander Madry. How does batch normalization help optimization? In *NeurIPS*, pages 2488–2498, 2018. [3](#)

[18] A. Sengupta, Y. Ye, R. Wang, C. Liu, and K. Roy. Going deeper in spiking neural networks: Vgg and residual architectures. *Frontiers in neuroscience*, 13, 2019. [1](#) [2](#) [3](#) [4](#) [6](#)

[19] K. Simonyan and A. Zisserman. Very deep convolutional networks for large-scale image recognition. *arXiv:1409.1556*, 2014. [6](#)

[20] V. Sze, Y.H. Chen, T.J. Yang, and J.S. Emer. Efficient processing of deep neural networks: A tutorial and survey. *Proceedings of the IEEE*, 105(12):2295–2329, 2019. [8](#)